Joint control of terrestrial gross primary productivity by plant phenology and physiology

Jianyang Xia[a,1,2], Shuli Niu[b,1,2], Philippe Ciais[c], Ivan A. Janssens[d], Jiquan Chen[e], Christof Ammann[f], Altaf Arain[g], Peter D. Blanken[h], Alessandro Cescatti[i], Damien Bonal[j], Nina Buchmann[k], Peter S. Curtis[l], Shiping Chen[m], Jinwei Dong[a], Lawrence B. Flanagan[n], Christian Frankenberg[o], Teodoro Georgiadis[p], Christopher M. Gough[q], Dafeng Hui[r], Gerard Kiely[s], Jianwei Li[a,t], Magnus Lund[u], Vincenzo Magliulo[v], Barbara Marcolla[w], Lutz Merbold[k], Leonardo Montagnani[x,y], Eddy J. Moors[z], Jørgen E. Olesen[aa], Shilong Piao[bb,cc], Antonio Raschi[dd], Olivier Roupsard[ee,ff], Andrew E. Suyker[gg], Marek Urbaniak[hh], Francesco P. Vaccari[dd], Andrej Varlagin[ii], Timo Vesala[jj,kk], Matthew Wilkinson[ll], Ensheng Weng[mm], Georg Wohlfahrt[nn,oo], Liming Yan[pp], and Yiqi Luo[a,qq,1,2]

[a]Department of Microbiology and Plant Biology, University of Oklahoma, Norman, OK 73019; [b]Synthesis Research Center of Chinese Ecosystem Research Network, Key Laboratory of Ecosystem Network Observation and Modeling, Institute of Geographic Sciences and Natural Resources Research, Beijing 100101, China; [c]Laboratoire des Sciences du Climat et de l'Environnement, 91191 Gif sur Yvette, France; [d]Department of Biology, University of Antwerpen, 2610 Wilrijk, Belgium; [e]Center for Global Change and Earth Observations and Department of Geography, Michigan State University, East Lansing, MI 48824; [f]Climate and Air Pollution Group, Federal Research Station Agroscope, CH-8046 Zurich, Switzerland; [g]School of Geography and Earth Sciences, McMaster University, Hamilton, ON, Canada L8S 4K1; [h]Department of Geography, University of Colorado, Boulder, CO 80302; [i]European Commission, Joint Research Center, Institute for Environment and Sustainability, 21027 Ispra, Italy; [j]Institut National de la Recherche Agronomique, UMR 1137 Institut National de la Recherche Agronomique–Université de Lorraine, 54280 Champenoux, France; [k]Institute of Agricultural Sciences, Eidgenössische Technische Hochschule Zurich, 8092 Zurich, Switzerland; [l]Department of Evolution, Ecology and Organismal Biology, The Ohio State University, Columbus, OH 43210; [m]State Key Laboratory of Vegetation and Environmental Change, Institute of Botany, Chinese Academy of Sciences, Beijing 100093, China; [n]Department of Biological Sciences, University of Lethbridge, Lethbridge, AB, Canada TIK 3M4; [o]Tropospheric sounding, assimilation, and modeling group, Jet Propulsion Laboratory, Pasadena, CA 91109; [p]Institute of Biometeorology, 40129 Bologna, Italy; [q]Department of Biology, Virginia Commonwealth University, Richmond, VA 23284-2012; [r]Department of Biological Sciences, Tennessee State University, Nashville, TN 37209; [s]Civil and Environmental Engineering Department and Environmental Research Institute, University College Cork, Cork, Ireland; [t]Department of Agriculture and Environmental Sciences, Tennessee State University, Nashville, TN 37209; [u]Department of Bioscience, Aarhus University, 4000 Roskilde, Denmark; [v]Institute for Mediterranean Agricultural and Forest Systems, National Research Council, 80040 Ercolano, Italy; [w]Sustainable Agro-Ecosystems and Bioresources Department, Fondazione Edmund Mach, 38010 S. Michele all'Adige, Italy; [x]Servizi Forestali, Provincia Autonoma di Bolzano, 39100 Bolzano, Italy; [y]Faculty of Science and Technology, Free University of Bolzano, 39100 Bolzano, Italy; [z]Earth System Science and Climate Change Group, Wageningen University and Research Centre, Wageningen UR, 6700 AA Wageningen, The Netherlands; [aa]Department of Agroecology, Aarhus University, DK-8830 Tjele, Denmark; [bb]Department of Ecology, College of Urban and Environmental Sciences, Peking University, Beijing 100871, China; [cc]Key Laboratory of Alpine Ecology and Biodiversity, Institute of Tibetan Plateau Research, Center for Excellence in Tibetan Earth Science, Chinese Academy of Sciences, Beijing 100085, China; [dd]Institute of Biometeorology, National Research Council, 50145 Florence, Italy; [ee]Cirad-Persyst, UMR Ecologie Fonctionnelle et Biogéochimie des Sols et des Agro-Ecosystémes, 34060 Montpellier, France; [ff]Tropical Agricultural Centre for Research and High Education, 7170 Turrialba, Costa Rica; [gg]School of Natural Resources, University of Nebraska, Lincoln, NE 68583-0961; [hh]Department of Meteorology, Poznan University of Life Sciences, 60649 Poznan, Poland; [ii]A. N. Severtsov Institute of Ecology and Evolution, Russian Academy of Sciences, Moscow, 119071, Russia; Departments of [jj]Physics and [kk]Forest Sciences, University of Helsinki, FIN-00014 Helsinki, Finland; [ll]Centre for Sustainable Forestry and Climate Change, Forest Research, Farnham GU10 4LH, United Kingdom; [mm]Department of Ecology and Evolutionary Biology, Princeton University, Princeton, NJ 08544; [nn]Institute of Ecology, University of Innsbruck, 6020 Innsbruck, Austria; [oo]Institute for Applied Remote Sensing and Institute for Alpine Environment, European Academy of Bolzano, 39100 Bolzano, Italy; [pp]School of Life Sciences, Fudan University, Shanghai 200433, China; and [qq]Center for Earth System Science, Tsinghua University, Beijing 100084, China

Terrestrial gross primary productivity (GPP) varies greatly over time and space. A better understanding of this variability is necessary for more accurate predictions of the future climate–carbon cycle feedback. Recent studies have suggested that variability in GPP is driven by a broad range of biotic and abiotic factors operating mainly through changes in vegetation phenology and physiological processes. However, it is still unclear how plant phenology and physiology can be integrated to explain the spatiotemporal variability of terrestrial GPP. Based on analyses of eddy–covariance and satellite-derived data, we decomposed annual terrestrial GPP into the length of the CO_2 uptake period (CUP) and the seasonal maximal capacity of CO_2 uptake (GPP_{max}). The product of CUP and GPP_{max} explained >90% of the temporal GPP variability in most areas of North America during 2000–2010 and the spatial GPP variation among globally distributed eddy flux tower sites. It also explained GPP response to the European heatwave in 2003 ($r^2 = 0.90$) and GPP recovery after a fire disturbance in South Dakota ($r^2 = 0.88$). Additional analysis of the eddy–covariance flux data shows that the interbiome variation in annual GPP is better explained by that in GPP_{max} than CUP. These findings indicate that terrestrial GPP is jointly controlled by ecosystem-level plant phenology and photosynthetic capacity, and greater understanding of GPP_{max} and CUP responses to environmental and biological variations will, thus, improve predictions of GPP over time and space.

ecosystem carbon uptake | growing season length | photosynthetic capacity | spatiotemporal variability | climate extreme

Large variability exists among estimates of terrestrial carbon sequestration, resulting in substantial uncertainty in modeled dynamics of atmospheric CO_2 concentration and predicted future climate change (1). The variability in carbon sequestration is partially caused by variation in terrestrial gross primary productivity (GPP) (2), which is the cumulative rate over time of gross plant

Significance

Terrestrial gross primary productivity (GPP), the total photosynthetic CO_2 fixation at ecosystem level, fuels all life on land. However, its spatiotemporal variability is poorly understood, because GPP is determined by many processes related to plant phenology and physiological activities. In this study, we find that plant phenological and physiological properties can be integrated in a robust index—the product of the length of CO_2 uptake period and the seasonal maximal photosynthesis—to explain the GPP variability over space and time in response to climate extremes and during recovery after disturbance.

photosynthesis at the ecosystem level. Plant photosynthesis has been successfully modeled at the biochemical level (3, 4). When leaf-level biochemical models of photosynthesis are scaled up to estimate annual GPP over a region and the globe, however, great uncertainty arises from both vegetation properties, such as biome-dependent leaf parameters (5, 6), and environmental factors, such as climate variability (7–9) and episodic disturbances (10–12). As a consequence, estimated present day global GPP varies from 105 to 177 Pg C y^{-1} in the fifth phase of the Coupled Model Intercomparison Project (13). Additionally, spatiotemporal patterns of GPP (2, 14), their responses to extreme climate events (12) and disturbances (10), and the underlying mechanisms are still not well-understood. Previous studies have indicated that vegetation properties and environmental factors shape annual GPP of an ecosystem directly or indirectly through affecting plant physiological activities (15) and/or phenology (16–21). Thus, integrating plant physiological and phenological properties may provide a unified approach to explain the variability of GPP over time and space and in response to disturbance.

In this study, we show that annual GPP in grams C meter^{-2} year^{-1}, the rate at which terrestrial ecosystems take up CO_2 from the atmosphere in a given year, can be quantitatively decomposed into

$$GPP = \alpha \cdot CUP \cdot GPP_{max}, \quad [1]$$

where the carbon dioxide uptake period (CUP; number of days per year) is a phenological indicator of the duration of ecosystem CO_2 assimilation within a given year. GPP$_{max}$ (grams C meter^{-2} day^{-1}) is

the maximal daily rate of gross photosynthesis during the CUP and represents a property of plant canopy physiology. The ratio between annual GPP and the product of CUP and GPP$_{max}$ is represented by α. We estimated α, CUP, and GPP$_{max}$ for 213 globally distributed terrestrial sites with daily GPP from the global network of micrometeorological tower sites (FLUXNET; La Thuile Database) (22) (*SI Appendix*, section S1.1.1 and Table S1) and all $0.1° \times 0.1°$ land grid cells in North America during 2000–2010 with an 8-d GPP product from the Moderate Resolution Imaging Spectroradiometer (MODIS) onboard the National Aeronautics and Space Administration Terra satellite (23) (*Materials and Methods*). Here, we show how CUP and GPP$_{max}$ jointly control the spatiotemporal variability of GPP and its response to and recovery from disturbances in different terrestrial ecosystems.

Results and Discussion

Using regression analysis, we first evaluated to what extent the product of CUP and GPP$_{max}$ (CUP × GPP$_{max}$) explained the variability of satellite-derived GPP over broad temporal and spatial scales. CUP × GPP$_{max}$ explained 94.9% of the interannual variability of the averaged MODIS GPP across North America from 2000 to 2010, with the minimum annual GPP (678 g C m^{-2} y^{-1}) in 2000 and the maximum (748 g C m^{-2} y^{-1}) in 2010 (Fig. 1A). The joint control of CUP and GPP$_{max}$ on the interannual variability of GPP was robust in most MODIS grid cells across North America but weak in tropical and Mediterranean climates, such as the
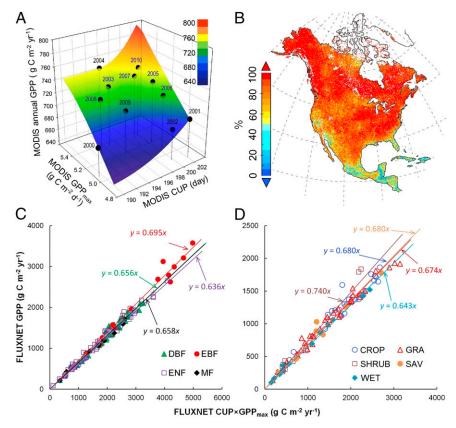

Fig. 1. Joint control of the temporal variability of satellite-derived annual GPP and the spatial variability of FLUXNET annual GPP by CUP and GPP$_{max}$. (*A*) The temporal variability of GPP in North America from 2000 to 2010 can be better understood by splitting annual GPP into GPP$_{max}$ and CUP. The flat color interpolated surface reflects a good relationship between annual GPP and GPP$_{max}$ × CUP ($R^2 = 0.95$, $P < 0.001$). Vertical lines were added to improve readability. (*B*) Contribution of GPP$_{max}$ × CUP to GPP temporal variability over 2000–2010. The contribution in each grid cell was derived from the R^2 in the linear regression analysis between GPP and GPP$_{max}$ × CUP. *C* and *D* show relationships between GPP and GPP$_{max}$ × CUP across FLUXNET sites in forest and nonforest biomes, respectively. Each data point in *C* and *D* represents one flux site with average data over different years. CROP, cropland; DBF, deciduous broadleaf forest; EBF, evergreen broadleaf forest; ENF, evergreen needleleaf forest; GRA, grassland; MF, mixed forest; SAV, savanna; SHRUB, shrubland; WET, wetland.

Caribbean region and California (Fig. 1B). Spatially, across all FLUXNET sites, although there was no relationship between CUP and GPP_{max} (*SI Appendix*, Fig. S1), CUP × GPP_{max} explained >95% of the spatial variation of annual observed GPP in all biomes (all $P < 0.001$) (Fig. 1 C and D).

The product of CUP and GPP_{max} also explains the impact of a climate extreme on ecosystem CO_2 uptake. Linear regression analysis showed that the GPP reduction caused by the European heatwave in 2003 (12) across FLUXNET sites was well-explained by CUP × GPP_{max} ($R^2 = 0.90$, $P < 0.001$) (Fig. 2A, Inset). However, CUP and GPP_{max} played different roles in heatwave-induced GPP reduction among sites. For example, the reduction in annual GPP mainly resulted from a decrease of GPP_{max} (−37%) for a beech forest in Sarrebourg, France but a shortening of CUP (−11%) for a spruce site in Tharandt, Germany (Fig. 2A).

We also analyzed the dynamics of satellite-derived annual GPP, CUP, and GPP_{max} during recovery from a wildfire that occurred on August 24, 2000 in the Black Hills National Forest in South Dakota (24) (*SI Appendix*, Fig. S2). Although GPP_{max} and CUP followed contrasting postfire trajectories, the recovery trajectory of annual GPP was well-captured by the product of CUP and GPP_{max} ($R^2 = 0.88$, $P < 0.001$) (Fig. 2B). Immediately after the fire, GPP was sharply reduced by 27% in 2001 (624 g C m^{-2} y^{-1}) and 26% in 2002 (636 g C m^{-2} y^{-1}) relative to GPP before the disturbance in 2000 (858 g C m^{-2} y^{-1}). Thereafter, annual GPP gradually recovered to 816 g C m^{-2} y^{-1} in 2010 (Fig. 2B). The dynamics of GPP_{max} after the fire paralleled those of annual GPP, with 40% and 36% reduction in 2001 and 2002, respectively, and then gradual recovery to 89% of prefire levels in 2010. In contrast, the CUP was extended by 30 to 60 days from 2000 (219 d) and then gradually shortened and returned to predisturbance values (Fig. 2B). The rapid extension of the CUP may have resulted from the return of grass in spring after fire disturbance (25).
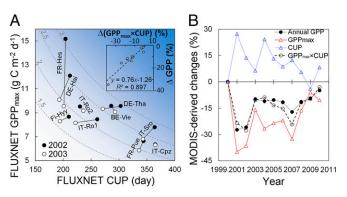

Fig. 2. Applications of the convergence of α (the ratio between annual GPP and GPP_{max} × CUP) to explain GPP response to and recovery from disturbances. (A) Determination of the annual GPP reduction during the European heatwave in 2003 (12) by GPP_{max} and CUP. The dashed hyperbolic curves represent constant values (shown near the curves) of GPP_{max} × CUP (kilograms C meter^{-2} year^{-1}), and the darker background blue color means a larger GPP_{max} × CUP. Inset shows the dependences of the relative changes in annual GPP (ΔGPP; percentage) in 2003 from those in 2002 on the relative changes in GPP_{max} × CUP [Δ(GPP_{max} × CUP); percentage] (black circles). The ten sites are: BE-Vie (Vielsalm, Belgium), DE-Hai (Hainich, Germany), DE-Tha (Tharandt, Germany), Fi-Hyy (Hyytiala, Finland), FR-Hes (Hesse Forest- Sarrebourg, France), FR-Pue (Puechabon, France), IT-Cpz (Castelporziano, Italy), IT-Ro1 and IT-Ro2 (Roccarespampani, Italy), IT-Sro (San Rossore, Italy). Detailed information about each FLUXNET site can be found in *SI Appendix*, Fig. S9 and Table S1. (B) Contrasting dynamics of GPP_{max} and CUP after an extensive wildfire in the Black Hills National Forest in South Dakota. The data were extracted from a burned 0.1° × 0.1° grid cell (43.85° N, 103.95° W) (original data are plotted in *SI Appendix*, Fig. S2). The ratio α was close to 0.62 during the 11-y span (*SI Appendix*, Fig. S10).

Not only did the product of CUP and GPP_{max} capture the variability in annual GPP over space and time and after disturbances, but the ratio α between annual GPP and CUP × GPP_{max} also converged across a broad range of vegetation types and environmental conditions (Fig. 3). The most frequent value of α was 0.62, with 90% of α-values falling within a range from 0.61 to 0.76 (Fig. 3A) based on an analysis of 213 FLUXNET sites. Those sites with $\alpha > 0.76$ were mainly located in tropical and subtropical climate zones (Fig. 3A and *SI Appendix*, Fig. S3). The analysis of the MODIS product showed a similar convergence of α over North America (Fig. 3B), with the most frequent value of 0.62 and a 90% range from 0.61 to 0.83. To explore the spatial distribution of α, we mapped the mean annual GPP, CUP, GPP_{max}, and α over 2000–2010. Although annual GPP, CUP, and GPP_{max} showed great spatial variability (*SI Appendix*, Fig. S4), α was relatively constant around 0.62 in most areas at a latitude of 37° N northward and gradually approached 1.0 toward the tropical regions of North America (Fig. 3C). Across North America, the temporal linear correlation between CUP × GPP_{max} and annual GPP was the highest in regions with α around 0.62 and gradually reduced with the ratio α approaching 1.0 (Fig. 3D).

High α-values were mainly distributed in tropical evergreen forest and regions with multiple growing seasons, where GPP_{max} and CUP exert weak controls over GPP variability (Fig. 3A, Inset). Values of α were high in tropical evergreen ecosystems, because GPP seasonality and amplitude were minimal, with plants assimilating CO_2 all year round. For example, daily GPP varied minimally across seasons in a tropical rain forest in Brazil (*SI Appendix*, Fig. S1.3.1), with α ranging between 0.77 and 0.80 from 2001 to 2003. The nontropical regions with high α-values usually have two or more peaks of daily GPP within a single year. For example, the Le Bray site in France, which is comprised of a maritime pine forest, had two separate GPP peaks in late May and September of 2005 (*SI Appendix*, Fig. S5). This phenomenon may also occur in Mediterranean regions with hot and dry summers (26) or double/triple cropping systems, where two or more crops are grown within a single year, such as winter wheat during winter and maize during summer in the North China Plain (27). Seasonally water-limited regions where two growing season peaks are present are widely distributed in the southern part of North America, leading to an abrupt increase in α at latitudes lower than about 30° N (Fig. 3C).

The decomposition of annual GPP into GPP_{max} and CUP allowed us to investigate the relative importance of GPP_{max} and CUP individually in regulating annual GPP variability among/within biomes (Fig. 4A). The linear correlation analysis across eight noncrop biomes showed that the biome-level GPP variability was significantly correlated to the variations in both GPP_{max} ($r^2 = 0.79$, $P = 0.003$) (Fig. 4B) and CUP ($r^2 = 0.64$, $P = 0.017$) (Fig. 4C). The partial correlation analysis across noncrop biomes revealed a larger contribution of GPP_{max} (partial $r^2 = 0.78$, $P = 0.004$) than CUP (partial $r^2 = 0.21$, $P < 0.001$) to GPP variability. A more important role of GPP_{max} than CUP in explaining the spatial variability of FLUXNET GPP was found within most biome types, including grassland (partial $r^2 = 0.70$, $P = 0.005$), shrubland (partial $r^2 = 0.52$, $P = 0.005$), savanna (partial $r^2 = 0.89$, $P = 0.001$), wetland (partial $r^2 = 0.91$, $P < 0.001$), and all forest types (partial $r^2 = 0.79$–0.87, all $P < 0.01$) (*SI Appendix*, Fig. S6 and Table S2). A recent analysis has found that temperature and precipitation changes impact the net primary productivity of woody plant ecosystems mainly through their effects on growing season length, standing biomass, and stand age (28). Thus, standing biomass and stand age might be very important determinants of GPP_{max} in forest ecosystems.

The joint control of GPP_{max} and CUP on GPP variability indicates that environmental changes influence annual GPP by simultaneously affecting vegetation phenology and photosynthetic capacity. For example, climate warming leads to greater ecosystem CO_2 uptake by extending CUP in most cold regions (7, 17, 29) but could reduce ecosystem CO_2 uptake when
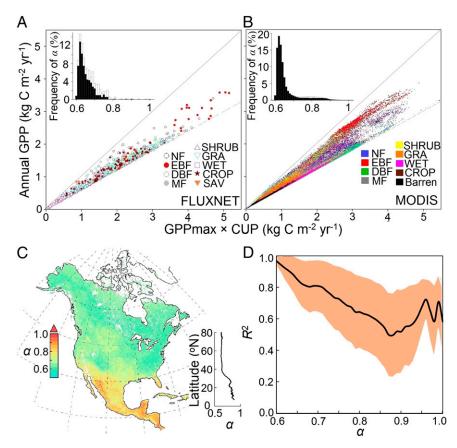
Xia et al.

Fig. 3. The relationship between annual GPP and the product of CUP and GPP$_{max}$ (i.e., α) from FLUXNET and satellite-derived data. The relationship between annual GPP and CUP × GPP$_{max}$ is shown across (A) all FLUXNET site-years and (B) all 0.1° × 0.1° land grids in North America. C shows spatial distributions of satellite-derived α, and D shows the relationship between α and the explanation of GPP$_{max}$ × CUP on temporal variability of annual GPP (R^2) (Fig. 1B) in North America. A, Inset and B, Inset show the relative frequency distribution of estimated α from all FLUXNET site-years and MODIS GPP data, respectively. The white bars are data from tropical and subtropical climate (including Mediterranean) zones and site-years with multiple GPP peaks, whereas the black bars are data from the rest of the site-years. C, Inset shows the latitudinal pattern of α with a 0.1° interval. CROP, cropland; DBF, deciduous broadleaf forest; EBF, evergreen broadleaf forest; GRA, grassland; NF, needleleaf forest; MF, mixed forest; SAV, savanna; SHRUB, shrubland; WET, wetland.

the GPP$_{max}$ is suppressed by the reduced snow melt water in spring (30, 31). Similarly, a recent analysis showed that warming-induced earlier springs reduced summer peak productivity during 1982–2008 in the North American boreal forests (32), which may have contributed to the declining trend of vegetation productivity associated with the climatic warming at northern high latitudes in the past few decades (33).

Given that simulated global GPP and its sensitivity to environmental factors vary substantially among current terrestrial biosphere models (13, 34), the findings in this study suggest that such uncertainty could largely stem from the different representations of vegetation phenology and photosynthetic capacity in the models. For example, although numerous vegetation phenology models have been developed for different biomes over the past few decades (35, 36), some existing terrestrial biosphere models poorly represent vegetation phenology in North America (8). Moreover, in those models, vegetation photosynthetic capacity may be unrealistically limited by the fixed parameterization of maximum rate of carboxylation (37), with observations indicating substantial temporal and spatial variations in maximum carboxylation (38, 39). Broadly collected vegetation phenology data derived from observations (40, 41), remote sensing (42, 43), and digital repeat photography (44, 45) as well as additional mechanistic understanding of canopy photosynthetic capacity (39, 46–48) could be useful to diagnose or benchmark model performances of simulating GPP (49).

Because the GPP$_{max}$ and CUP estimates were derived from existing data, our approach cannot be used for GPP prediction

unless GPP$_{max}$ and CUP can be inferred from other indicators. We first examined whether GPP$_{max}$ derived from MODIS GPP data was comparable with that measured by the flux towers in North America. We found that, although the two datasets had different spatial and temporal scales, the GPP$_{max}$ estimates from MODIS data were close to those from FLUXNET data at most sites with low GPP$_{max}$ (*SI Appendix*, Fig. S7). The FLUXNET data had much higher GPP$_{max}$ than MODIS data, mainly in the cropland sites with high GPP$_{max}$ (*SI Appendix*, Fig. S7). In addition to FLUXNET data, the maximum monthly sun-induced chlorophyll fluorescence data could be useful to estimate GPP$_{max}$ globally (50). We also examined whether the MODIS-derived CUP can be inferred from other types of satellite-derived datasets, such as the daily record of freeze/thaw status across North America (*SI Appendix*, section 1.8). We found that the MODIS-derived CUP is strongly correlated with the photosynthetically active period estimated from the freeze/thaw status data at most latitudes (*SI Appendix*, Fig. S8). The freeze/thaw status data can only provide information where the soil actually freezes in winter, partially leading to the disagreement between the two datasets in tropical regions (*SI Appendix*, Fig. S8). Thus, Eq. **1** could be useful for estimating and predicting annual GPP if both CUP and GPP$_{max}$ can be inferred from biotic and abiotic drivers measured at a global scale, the topic of a substantial body of ongoing research (15, 51).

In summary, we found a simple proximate cause to explain variation in annual GPP (i.e., Eq. **1**) over space and time, in response to a climate extreme, and during recovery after disturbance.
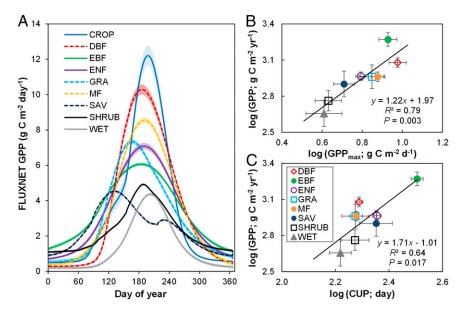
ECOLOGY

Fig. 4. (*A*) Dynamic of daily GPP in different biomes based on the FLUXNET dataset. The curves are obtained by averaging daily GPP over all site-years of each biome type, with the shaded areas representing SEs on GPP. *B* and *C* show dependence of annual FLUXNET GPP variability on GPP$_{max}$ and CUP, respectively, among biomes. Note that cropland was excluded in the correlation analyses. Note that there were, in total, 12 EBF sites in this analysis, and 7 of them were distributed in the temperate zone according to the MODIS IGBP (International Geosphere-Biosphere Programme) land cover classification (glcf.umd.edu/data/lc/) (*SI Appendix*, Table S1). CROP, cropland; DBF, deciduous broadleaf forest; EBF, evergreen broadleaf forest; ENF, evergreen needleleaf forest; GRA, grassland; MF, mixed forest; SAV, savanna; SHRUB, shrubland; WET, wetland.

The representation of interannual and spatial variations in GPP by the product of CUP and GPP$_{max}$ was strong in those ecosystems with α-values close to 0.62 but weaker toward the tropics or in seasonally water-limited regions, where α-values approached 1.0. The strong correlation of annual GPP with the product of CUP and GPP$_{max}$ in several different ecosystem types may be useful in detecting shifts in vegetation state and for monitoring short- and long-term response of GPP to extreme climate conditions and disturbances. Given that GPP$_{max}$ better explains GPP variability than CUP, future studies need to emphasize the regulatory mechanisms for the dynamics of ecosystem photosynthetic capacity in terrestrial ecosystems.

Materials and Methods

GPP estimates (positive GPP means CO_2 uptake) from 213 FLUXNET sites from the La Thuile Database (www.fluxdata.org/default.aspx) (*SI Appendix*, Table S1) and the MODIS aboard National Aeronautics and Space Administration Terra satellites (MOD17A2 GPP) (23) were used in the analyses (*SI Appendix*, section S1.1). For FLUXNET sites, only those site-years with >300 daily estimates were chosen from the database. Because the MODIS GPP product was well-evaluated in North America (52), we only performed our analysis on MODIS GPP in this region from 2000 to 2010.

The determinations of CUP and GPP$_{max}$ were from the method introduced by Gu et al. (53, 54) (*SI Appendix*, section S1.2). The CUP, GPP$_{max}$, and the ratio between annual GPP and CUP × GPP$_{max}$ (i.e., α) were estimated for each selected FLUXNET site and each 0.1° × 0.1° land grid cell of the MODIS product by the following steps (*SI Appendix*, section S1.3). (*i*) We judged if the site-year or grid cell is evergreen or not by counting the number of days with larger daily GPP than a given value (a site or land grid cell was defined as evergreen if there were more than 360 d with daily GPP > 1 g C m^{-2} d^{-1} within 1 y). (*ii*) The number of seasons in the nonevergreen site-years or land grid cells was determined by a model function (*SI Appendix*, section S1.3 and Eq. S6) suggested by the TIMESAT software (55). For those site-years and grid cells with one season, we fitted a five-parameter Weibull function to the data from that year. For those site-years or land grid cells with more than one season, we fitted the Weibull function to each season.

The nonlinear data fitting was performed with the function nls in R (www.r-project.org/) (*SI Appendix*, section S1.4). The robustness of the method was carefully validated by various approaches, including an evaluation with the data from all long-term FLUXNET sites (*SI Appendix*, section S1.5), a parameter sensitivity analysis of the Weibull function (*SI Appendix*, section S1.6), and a

random resampling test of the Weibull function (*SI Appendix*, section S1.7). Linear regression analysis was used to examine the contribution of CUP × GPP$_{max}$ to the temporal and spatial variations of annual GPP. The global daily record of landscape freeze/thaw data from January 1, 2000 to December 31, 2010 was analyzed for an additional indicator of CUP (*SI Appendix*, section S1.8).

To further identify the relative contribution of GPP$_{max}$ and CUP to GPP variability, we first linearized Eq. **1** by replacing all variables with their logarithms (base 10) as

$$\log(GPP) = \log(\alpha) + \log(CUP) + \log(GPP_{max}). \quad [2]$$

Then, we applied the partial correlation analysis to examine the relative contributions of CUP and GPP$_{max}$ to FLUXNET GPP variability among and within biomes.

1. Graven HD, et al. (2013) Enhanced seasonal exchange of CO_2 by northern ecosystems since 1960. *Science* 341(6150):1085–1089.
2. Jung M, et al. (2012) Global patterns of land-atmosphere fluxes of carbon dioxide, latent heat, and sensible heat derived from eddy covariance, satellite, and meteorological observations. *J Geophys Res Biogeosci* 116:G00J07.
3. Farquhar GD, von Caemmerer S, Berry JA (1980) A biochemical model of photosynthetic CO_2 assimilation in leaves of C_3 species. *Planta* 149(1):78–90.
4. Collatz GJ, Ribas-Carbo M, Berry J (1992) Coupled photosynthesis-stomatal conductance model for leaves of C_4 plants. *Funct Plant Biol* 19(5):519–538.
5. Reich PB, Walters MB, Ellsworth DS (1992) Leaf life-span in relation to leaf, plant, and stand characteristics among diverse ecosystems. *Ecol Monogr* 62(3):365–392.
6. Cramer W, et al. (1999) Comparing global models of terrestrial net primary productivity (NPP): Overview and key results. *Glob Chang Biol* 5(S1):1–15.
7. Xia JY, et al. (2014) Terrestrial carbon cycle affected by non-uniform climate warming. *Nat Geosci* 7(3):173–180.
8. Richardson AD, et al. (2012) Terrestrial biosphere models need better representation of vegetation phenology: Results from the North American Carbon Program Site Synthesis. *Glob Chang Biol* 18(2):566–584.
9. Bellenger H, Guilyardi E, Leloup J, Lengaigne M, Vialard J (2014) ENSO representation in climate models: From CMIP3 to CMIP5. *Clim Dyn* 42(7-8):1999–2018.
10. Amiro BD, et al. (2010) Ecosystem carbon dioxide fluxes after disturbance in forests of North America. *J Geophys Res Biogeosci* 115(G4):G00K02.
11. Running SW (2008) Climate change. Ecosystem disturbance, carbon, and climate. *Science* 321(5889):652–653.
12. Ciais P, et al. (2005) Europe-wide reduction in primary productivity caused by the heat and drought in 2003. *Nature* 437(7058):529–533.
13. Anav A, et al. (2013) Evaluating the land and ocean components of the global carbon cycling in the CMIP5 Earth System Models. *J Clim* 26:6801–6843.
14. Beer C, et al. (2010) Terrestrial gross carbon dioxide uptake: Global distribution and covariation with climate. *Science* 329(5993):834–838.
15. Stoy PC, Trowbridge AM, Bauerle WL (2014) Controls on seasonal patterns of maximum ecosystem carbon uptake and canopy-scale photosynthetic light response: Contributions from both temperature and photoperiod. *Photosynth Res* 119(1-2):49–64.
16. Xia J, Wan S (2012) The effects of warming-shifted plant phenology on ecosystem carbon exchange are regulated by precipitation in a semi-arid grassland. *PLoS ONE* 7(2):e32088.
17. Piao S, Friedlingstein P, Ciais P, Viovy N, Demarty J (2007) Growing season extension and its impact on terrestrial carbon cycle in the Northern Hemisphere over the past 2 decades. *Global Biogeochem Cycles* 21(3):GB3018.
18. Richardson AD, et al. (2010) Influence of spring and autumn phenological transitions on forest ecosystem productivity. *Philos Trans R Soc Lond B Biol Sci* 365(1555):3227–3246.
19. Keenan TF, et al. (2014) Net carbon uptake has increased through warming-induced changes in temperate forest phenology. *Nat Clim Chang* 4:598–604.
20. Churkina G, Schimel D, Braswell BH, Xiao X (2005) Spatial analysis of growing season length control over net ecosystem exchange. *Glob Chang Biol* 11(10):1777–1787.
21. Dragoni D, et al. (2011) Evidence of increased net ecosystem productivity associated with a longer vegetated season in a deciduous forest in south-central Indiana, USA. *Glob Chang Biol* 17(2):886–897.
22. FLUXNET Synthesis Dataset (La Thuile 2007). Available at www.fluxdata.org/default.aspx. Accessed January 2014.
23. Heinsch FA, et al. (2003) *GPP and NPP (MOD17A2/A3) Products NASA MODIS Land Algorithm. MOD17 User's Guide*. Available at datamirror.csdb.cn/modis/resource/doc/MOD17_UsersGuide.pdf. Accessed November 2013.
24. Xiao X, Biradar C, Wang A, Sheldon S, Chen Y (2011) Recovery of vegetation canopy after severe fire in 2000 at the Black Hills National Forest, South Dakota, USA. *J Resour Ecol* 2(2):106–116.
25. Lentile LB, Smith FW, Shepperd WD (2005) Patch structure, fire-scar formation, and tree regeneration in a large mixed-severity fire in the South Dakota Black Hills, USA. *Can J For Res* 35(12):2875–2885.
26. Giorgi F, Lionello P (2008) Climate change projections for the Mediterranean region. *Glob Planet Change* 63(2-3):90–104.
27. Liu XJ, Ju XT, Zhang FS, Pan JR, Christie P (2003) Nitrogen dynamics and budgets in a winter wheat-maize cropping system in the North China Plain. *Field Crops Res* 83(2):111–124.
28. Michaletz ST, Cheng D, Kerkhoff AJ, Enquist BJ (2014) Convergence of terrestrial plant production across global climate gradients. *Nature* 512(7512):39–43.
29. Schwartz MD, Ahas R, Aasa A (2006) Onset of spring starting earlier across the Northern Hemisphere. *Glob Chang Biol* 12(2):343–351.
30. Sacks WJ, Schimel DS, Monson RK (2007) Coupling between carbon cycling and climate in a high-elevation, subalpine forest: A model-data fusion analysis. *Oecologia* 151(1):54–68.
31. Hu J, Moore DJP, Burns SP, Monson RK (2010) Longer growing seasons lead to less carbon sequestration by a subalpine forest. *Glob Chang Biol* 16(2):771–783.
32. Buermann W, Bikash PR, Jung M, Burn DH, Reichstein M (2013) Earlier springs decrease peak summer productivity in North American boreal forests. *Environ Res Lett* 8(2):024027.
33. Jeong SJ, Ho CH, Kim BM, Feng S, Medvigy D (2013) Non-linear response of vegetation to coherent warming over northern high latitudes. *Remote Sens Lett* 4(2):123–130.
34. Piao S, et al. (2013) Evaluation of terrestrial carbon cycle models for their response to climate variability and to CO_2 trends. *Glob Chang Biol* 19(7):2117–2132.
35. White MA, Thornton PE, Running SW (1997) A continental phenology model for monitoring vegetation responses to interannual climatic variability. *Global Biogeochem Cycles* 11(2):217–234.
36. Hodges T (1990) *Predicting Crop Phenology* (CRC, Boston).
37. Bonan GB, et al. (2011) Improving canopy processes in the Community Land Model version 4 (CLM4) using global flux fields empirically inferred from FLUXNET data. *J Geophys Res Biogeosci* 116(G2):G02014.
38. Xu L, Baldocchi DD (2003) Seasonal trends in photosynthetic parameters and stomatal conductance of blue oak (Quercus douglasii) under prolonged summer drought and high temperature. *Tree Physiol* 23(13):865–877.
39. Kattge J, Knorr W, Raddatz T, Wirth C (2008) Quantifying photosynthetic capacity and its relationship to leaf nitrogen content for global-scale terrestrial biosphere models. *Glob Change Biol* 15(4):976–991.
40. Dierenbach J, Badeck FW, Schaber J (2013) The plant phenological online database (PPODB): An online database for long-term phenological data. *Int J Biometeorol* 57(5):805–812.
41. Wolkovich EM, et al. (2012) Warming experiments underpredict plant phenological responses to climate change. *Nature* 485(7399):494–497.
42. Zhang X, et al. (2003) Monitoring vegetation phenology using MODIS. *Remote Sens Environ* 84(3):471–475.
43. Jones MO, Jones LA, Kimball JS, McDonald KC (2011) Satellite passive microwave remote sensing for monitoring global land surface phenology. *Remote Sens Environ* 115(4):1102–1114.
44. Richardson AD, et al. (2007) Use of digital webcam images to track spring green-up in a deciduous broadleaf forest. *Oecologia* 152(2):323–334.
45. Keenan TF, et al. (2014) Tracking forest phenology and seasonal physiology using digital repeat photography: A critical assessment. *Ecol Appl* 24(6):1478–1489.
46. Zhang Y, et al. (2014) Estimation of vegetation photosynthetic capacity from space-based measurements of chlorophyll fluorescence for terrestrial biosphere models. *Glob Chang Biol* 20(12):3727–3742.
47. Joiner J, et al. (2013) Global monitoring of terrestrial chlorophyll fluorescence from moderate spectral resolution near-infrared satellite measurements: Methodology, simulations, and application to GOME-2. *Atmos Meas Tech Discuss* 6(2):3883–3930.
48. Zhu Z, et al. (2013) Global data sets of vegetation leaf area index (LAI) 3g and Fraction of Photosynthetically Active Radiation (FPAR) 3g derived from Global Inventory Modeling and Mapping Studies (GIMMS) Normalized Difference Vegetation Index (NDVI3g) for the period 1981 to 2011. *Remote Sens (Basel)* 5(2):927–948.
49. Luo YQ, et al. (2012) A framework for benchmarking land models. *Biogeosciences* 9(10):3857–3874.
50. Guanter L, et al. (2014) Global and time-resolved monitoring of crop photosynthesis with chlorophyll fluorescence. *Proc Natl Acad Sci USA* 111(14):E1327–E1333.
51. Koster R, Walker G, Collatz G, Thornton P (2014) Hydroclimatic controls on the means and variability of vegetation phenology and carbon uptake. *J Clim* 27:5632–5652.
52. Heinsch FA, et al. (2006) Evaluation of remote sensing based terrestrial productivity from MODIS using regional tower eddy flux network observations. *IEEE Trans Geosci Remote Sens* 44(7):1908–1925.
53. Gu L, et al. (2003) *Phenology of Vegetation Photosynthesis. Phenology: An Integrative Environmental Science* (Springer, New York), pp 467–485.
54. Gu L, et al. (2009) *Characterizing the Seasonal Dynamics of Plant Community Photosynthesis Across a Range of Vegetation Types. Phenology of Ecosystem Processes* (Springer, New York), pp 35–58.
55. Eklundh L, Jönsson P (2012) *Timesat 3.1 Software Manual*.

ECOLOGY